AFRL-RQ-WP-TR-2018-0014

STRUCTURAL SCALE MODELING AND EXPERIMENTS FOR HYPERSONIC VEHICLES

Timothy J. Beberniss and Thomas G. Eason, III

Hypersonic Sciences Branch
High Speed Systems Division

OCTOBER 2017
Final Report

AIR FORCE RESEARCH LABORATORY
AEROSPACE SYSTEMS DIRECTORATE
WRIGHT-PATTERSON AIR FORCE BASE, OH 45433-7542
AIR FORCE MATERIEL COMMAND
UNITED STATES AIR FORCE

NOTICE AND SIGNATURE PAGE

Using Government drawings, specifications, or other data included in this document for any purpose other than Government procurement does not in any way obligate the U.S. Government. The fact that the Government formulated or supplied the drawings, specifications, or other data does not license the holder or any other person or corporation; or convey any rights or permission to manufacture, use, or sell any patented invention that may relate to them.

This report was cleared for public release by the USAF 88th Air Base Wing (88 ABW) Public Affairs Office (PAO) and is available to the general public, including foreign nationals.

Copies may be obtained from the Defense Technical Information Center (DTIC) (http://www.dtic.mil).

AFRL-RQ-WP-TR-2018-0014 HAS BEEN REVIEWED AND IS APPROVED FOR PUBLICATION IN ACCORDANCE WITH ASSIGNED DISTRIBUTION STATEMENT.

*//Signature//

TIMOTHY J. BEBERNISS
Program Manager
Hypersonic Sciences Branch
High Speed Systems Division

//Signature//

MICHAEL S. BROWN, Chief
Hypersonic Sciences Branch
High Speed Systems Division
Aerospace Systems Directorate

//Signature//

JAMES H. MILLER
Principal Advisor
High Speed Systems Division
Aerospace Systems Directorate

This report is published in the interest of scientific and technical information exchange, and its publication does not constitute the Government's approval or disapproval of its ideas or findings.

*Disseminated copies will show "//Signature//" stamped or typed above the signature blocks.

REPORT DOCUMENTATION PAGE

Form Approved
OMB No. 0704-0188

1. REPORT DATE *(DD-MM-YY)*	2. REPORT TYPE	3. DATES COVERED *(From - To)*
October 2017	Final	02 October 2014 – 02 October 2017

4. TITLE AND SUBTITLE
STRUCTURAL SCALE MODELING AND EXPERIMENTS FOR HYPERSONIC VEHICLES

5a. CONTRACT NUMBER
In-house

5b. GRANT NUMBER

5c. PROGRAM ELEMENT NUMBER
61102F

6. AUTHOR(S)
Timothy J. Beberniss and Thomas G. Eason, III

5d. PROJECT NUMBER
3002

5e. TASK NUMBER
N/A

5f. WORK UNIT NUMBER
Q1FF

7. PERFORMING ORGANIZATION NAME(S) AND ADDRESS(ES)
Hypersonic Sciences Branch (AFRL/RQHF)
High Speed Systems Division
Air Force Research Laboratory, Aerospace Systems Directorate
Wright-Patterson Air Force Base, OH 45433-7542
Air Force Materiel Command, United States Air Force

8. PERFORMING ORGANIZATION REPORT NUMBER
AFRL-RQ-WP-TR-2018-0014

9. SPONSORING/MONITORING AGENCY NAME(S) AND ADDRESS(ES)
Air Force Research Laboratory
Aerospace Systems Directorate
Wright-Patterson Air Force Base, OH 45433-7542
Air Force Materiel Command
United States Air Force

10. SPONSORING/MONITORING AGENCY ACRONYM(S)
AFRL/RQHF

11. SPONSORING/MONITORING AGENCY REPORT NUMBER(S)
AFRL-RQ-WP-TR-2018-0014

12. DISTRIBUTION/AVAILABILITY STATEMENT
DISTRIBUTION STATEMENT A: Approved for public release. Distribution is unlimited.

13. SUPPLEMENTARY NOTES
PA Case Number: 88ABW-2018-0600; Clearance Date: 09 Feb 2018.

14. ABSTRACT
A fundamental and multifaceted approach toward improving the communities understanding of structural response in high-speed environments was devised. This includes careful spatial and temporal characterization of the driving force exerted by flow in the form of pressure and heating as well as the structural resistance characterized by deflections and temperatures.

15. SUBJECT TERMS
structural, panel flutter, hypersonic, pressure sensitive paint, temperature sensitive paint, digital image correlation, flow characterization, incident shock, impingement

16. SECURITY CLASSIFICATION OF:			17. LIMITATION OF ABSTRACT:	18. NUMBER OF PAGES	19a. NAME OF RESPONSIBLE PERSON (Monitor)
a. REPORT	b. ABSTRACT	c. THIS PAGE			Timothy J. Beberniss
Unclassified	Unclassified	Unclassified	SAR	29	19b. TELEPHONE NUMBER *(Include Area Code)* N/A

Table of Contents

Section **Page**

List of Figures

Figure **Page**

1. INTRODUCTION

The United States Air Force has a logistical and tactical need for reusable hypersonic air vehicles. Hypersonic flight involves speeds of Mach 5 and greater. Initial investigations have shown that the region of Mach 5 to 6 is of particular interest for reusable manned vehicles [1]. At these lower hypersonic speeds large acreage regions of the vehicle can be designed with more traditional techniques of thin skin and stringer stiffeners.

To withstand the high-speed fluctuating pressure and the 1000 °F heating from skin friction, the thin skin could be constructed from a metallic such as titanium. These more traditional structural designs and materials are fairly well understood; however, certain phenomena, such as shock impingement and panel thermal buckling combined with dynamic snap-through, lack sufficient predictive capabilities and the experimental data to validate the required methods.

The U.S. Air Force Research Laboratory Structural Sciences Center has been involved in a series of high-speed fluid-structure interaction experiments in a Mach 2 wind tunnel. The experiments are intended to recreate an environment a high-speed aircraft structure would encounter. Experimental ground-based testing of environments that high-speed aircraft encounter was prohibitively expensive or not possible to create. Therefore, the experiments took advantage of many new and novel high-speed full-field measurement techniques that would not be an option for a flight test. The desire for the full-field measurements stems from the complex nature of the loading and resulting nonlinear vibration response.

Accelerometers mass load the lightly damped skin structure, and there is a limit on the number of simultaneous measurement points using non-contact laser Doppler velocimetry. Various configurations of baseline, shock impingement, and thermal buckling load conditions were explored and initial results are also presented in this report.

The ultimate goal of the experiment is to dynamically snap-through a buckled panel with an impinged shockwave to induce high cycle fatigue failure. This combined loading environment is intended to represent and better understand a worst-case scenario for a hypersonic vehicle outer mold line structure.

The overall objective for this work is to devise a fundamental and multifaceted approach toward improving the communities understanding of structural response in high speed environments. This includes careful spatial and temporal characterization of the driving force exerted by flow in the form of pressure and heating as well as the structural resistance characterized by deflections and temperatures. To support this objective, the following three main tasks were undertaken:

(a) Benchmark Challenge Problems - Develop relevant, experimental fluid-thermal-structural benchmark challenge problems, provide open-source validation-quality experimental data sets, and extend in-house novel full-field dynamic experimental techniques to explore multi-discipline phenomena for extreme environment structures that serve as the basis for establishing the capabilities of, and requirements for, fully coupled analysis methods.

(b) Coupled Modeling Methods - Develop fundamental knowledge to identify the requirements for variable-fidelity and variable-scale fluid-thermal-structural coupling, and the characteristics of the methods necessary to predict the response and life of a structure undergoing transient and dynamic extreme-environment loading.

(c) Enabling Long-Duration Time-Record Simulations - Develop methods that enable long-duration time-record simulations that include transient and localized effects essential for the modeling and prediction of structural response, flaws and damage of hypersonic vehicle structures.

2. EXPERIMENTAL SETUP

The main accomplishment for the period of performance was completing the test matrix for fluid structure interaction experiment in Research Cell 19 (RC-19) in the summer of 2016. Originally, the thin panel test was to be accomplished in calendar year 2015, but one of the large air compressors went down, postponing the test. The extra time was used to explore full field temperature measurement capability and the feasibility of combining pressure sensitive paint (PSP) and temperature sensitive paint (TSP) into a single test simultaneous full field measurement.

The test plan executed included a rigid control blank, as well as the thin panel. A rigid control specimen was instrumented for transient pressure measurement. The basic setup for the experiment was maintained from the previous work by the authors in the high-speed wind tunnel RC-19 [2-4]. The most significant changes include the upgrade to four SA-Z Photron high-speed cameras for the 3D digital image correlation (DIC) vibration measurement of the flexible panel from the back non-flow side, and the fast-reacting PSP for full-field dynamic pressure of the panel flow side. Additional measurements of TSP for full-field flexible panel temperature measurement from the front flow side, and the high-speed shadowgraph to measure the dynamic motion of the shock impingement were included to more completely characterize the environment.

Much of the measurement equipment can be seen surrounding the wind tunnel test section in **Figure 1a**. Two of the SA-5 high-speed cameras used in the previous tests [2 through 4] were utilized in one set of experiments in place of the PSP/TSP camera to also conduct DIC vibration measurements of the flexible panel from the front flow side as seen in **Figure 1b**. The front side DIC was filmed through a front surface mirror angled at exactly 45 degrees under the tunnel test section. The two simultaneous DIC measurements (front and back) were then compared to explore the effects of high-speed flow density gradients created by shockwaves on DIC results. All experiments were run at a tunnel flow speed of Mach 2 and a stagnation pressure of 50 psi. Five shock impingement conditions were explored, including no shock, panel 1/2 length point, 1/4 length point, 1/8 length point, and panel leading edge. All high-speed cameras were synchronized and sampled at 5,000 frames per second.

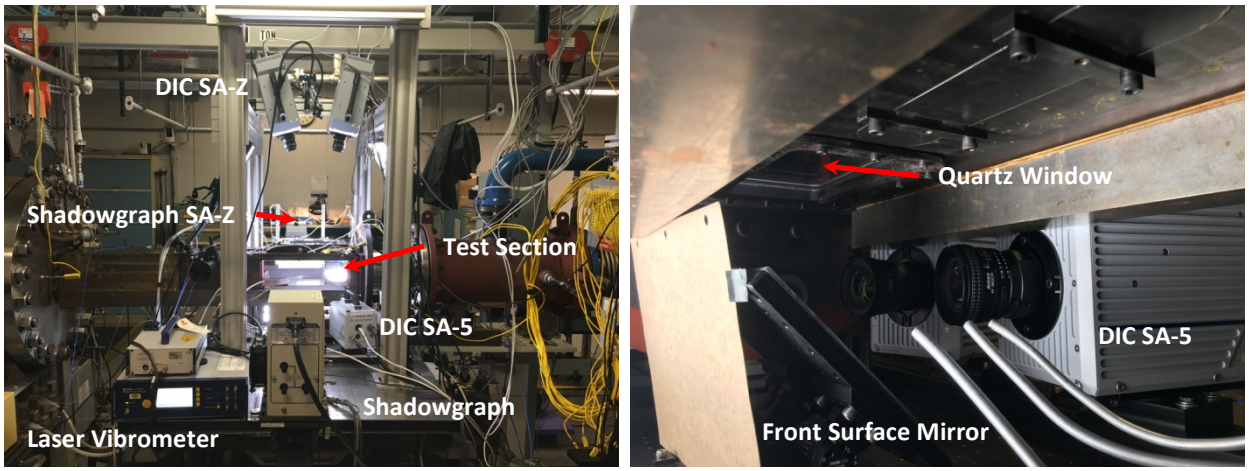

Figure 1. RC-19 Fluid-structure Interaction
a) general setup and b) DIC vibration measurement through the shockwave

3. RESULTS

3.1. Flow Characterization

Characterization of the flow of the basic RC-19 Mach 2 configuration used for the current fluid-structure interaction series of tests was originally conducted in the 90's when the tunnel was first constructed [5]. Considering both the top and bottom walls had been redesigned and constructed with several joints not present in the original design, it was decided that boundary layer characterization should be revisited. A pitot tube, which was connected to a stepper motor, was designed and constructed (**Figure 2**). Three locations of pitot tube pressure data were taken in the stream wise and cross flow directions. The boundary layer growth in the flow direction should be spatially linear; therefore, one location near the panel leading edge and another near the panel trailing edge were used to collect boundary layer pressure data. Another location near the tunnel sidewall was used to help characterize the 3D wall effects on the boundary layer. At each of the locations, the stepper motor was used to collect pressure data at locations vertically into the flow from the top wall to 0.75 inch into the core flow.

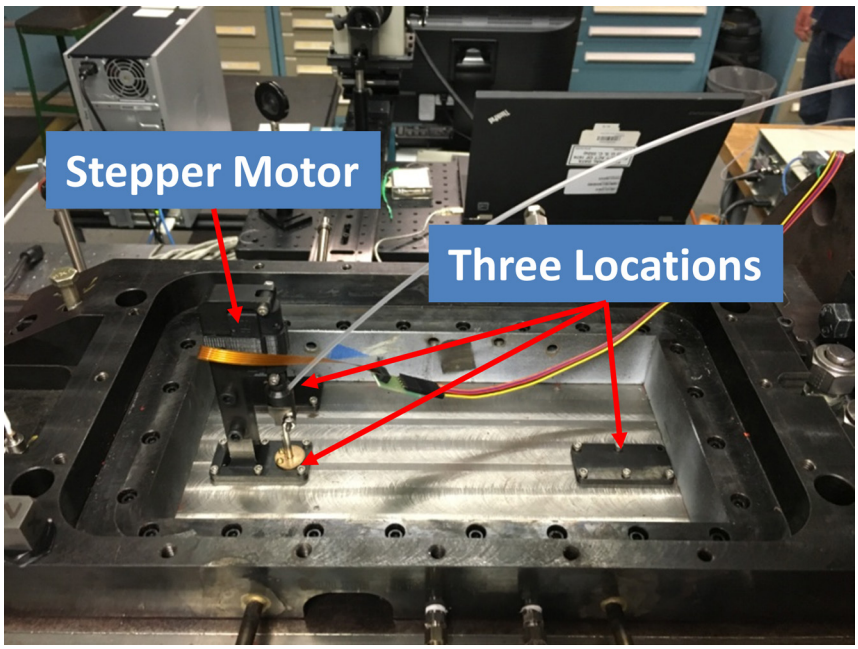

Figure 2. Tunnel Boundary Layer Characterization Test Setup

To investigate the effects of the sharp density gradients of shockwaves on panel response, the motion of the shockwave itself needs to be investigated. The shockwave was visualized using shadowgraph techniques and filmed with one of the SA-Z high-speed cameras (**Figure 1**). A single image of the shadowgraph image series can be seen in **Figure 3**. The complete time history of images were then run through image processing software utilizing the MATLAB image processing toolbox. The change in grayscale value of a pixel of interest was tracked over time and then transferred into the frequency domain to interrogate the dynamic behavior of the shock motion. A pixel grayscale PSD of the shock oscillation results can be seen in **Figure 4**. The red line is the grayscale variation at a point in the shadowgraph image where no shockwave is present and can be considered the background or noise floor of the measurement. The blue line is a pixel on the incident shockwave near the center of the test section and the black line is a pixel on the reflected shockwave downstream.

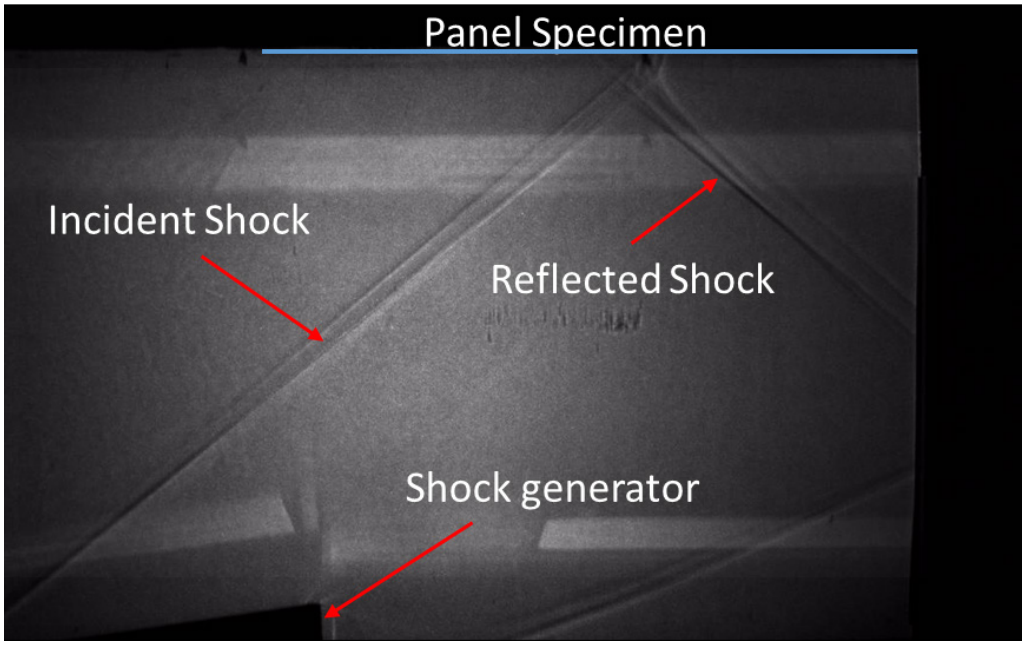

Figure 3. High-speed Shadowgraph Image of Incident Shock and Reflected Shockwave

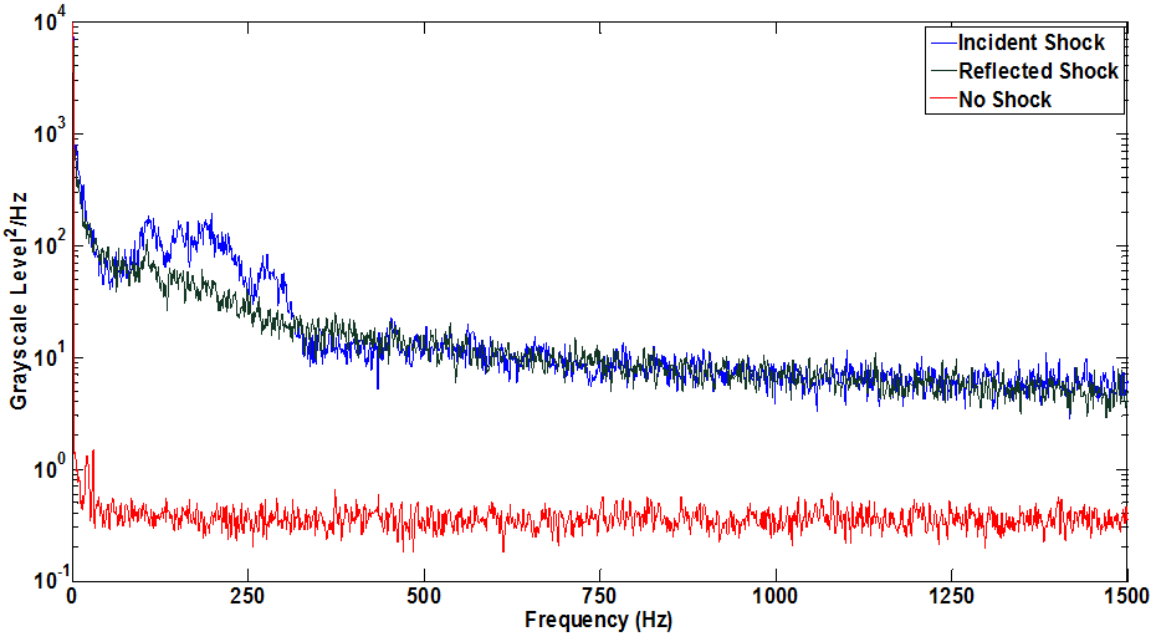

Figure 4. High-speed Shadowgraph PSD

(▬) no shock, (▬) incident shock, and (▬) reflected shockwave

It can be seen that, in general, the dynamic content of a pixel on a shockwave is much higher than the pixel in free stream. The dynamic content of the shockwave increases at lower frequencies until, at very low frequencies, the content increases dramatically. This dramatic increase in motion at low frequencies is the large shock motion that is typically seen in real-time. The incident shock has some distinct peaks in the PSD between about 100 and 350 Hz. This same dynamic content can be seen in high-speed PSP pressure data (**Figure 5**). The blank nonflexible specimen with no shock present qualitatively shows

almost identical frequency content between 100 Hz and 350 Hz which would indicate it is in general the dynamics of the RC-19 boundary layer. The incident shock motion is therefore largely dictated by the dynamics of the upstream turbulent boundary layer.

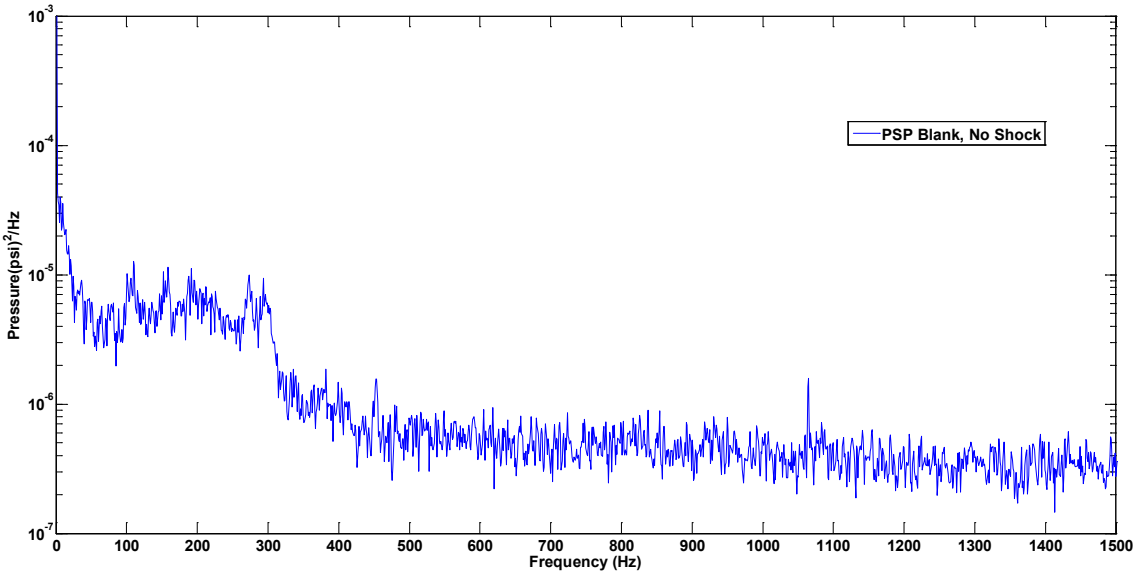

Figure 5. High-speed PSP of Blank Specimen with No Shock

3.2. Full Field Pressure

PSP results of the four main shock impingement test cases can be seen in **Figure 1.** Shown in the figure is a single image from the sequence of high speed images to illustrate spatial pressure distribution.

a)

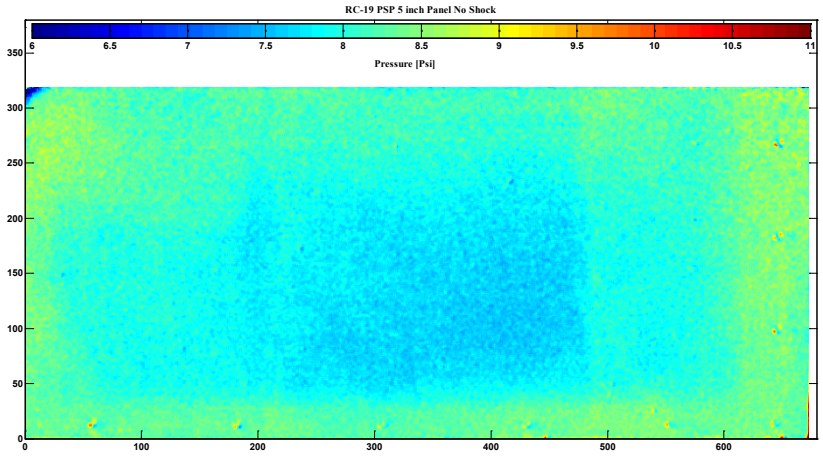

b)

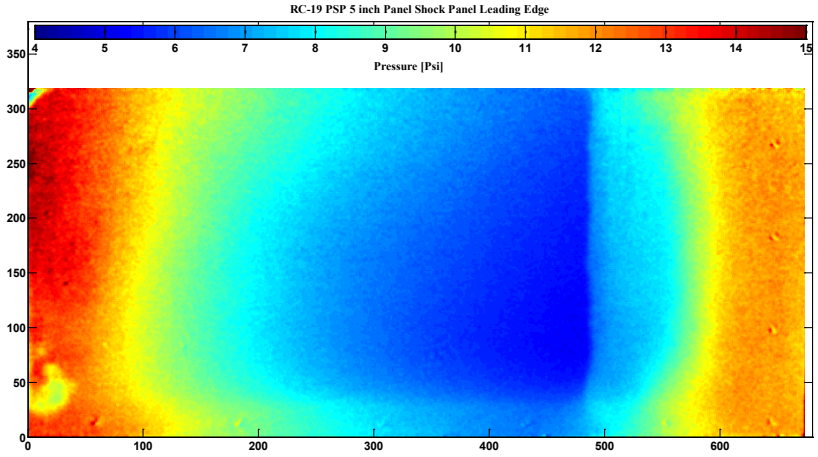

c)

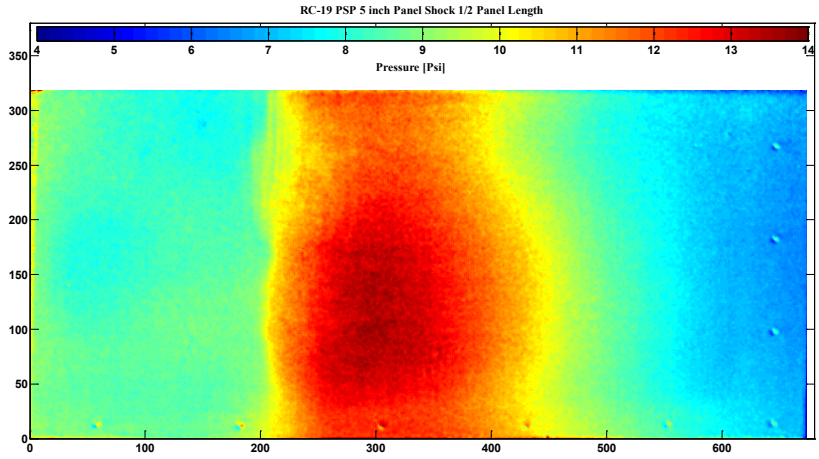

d)

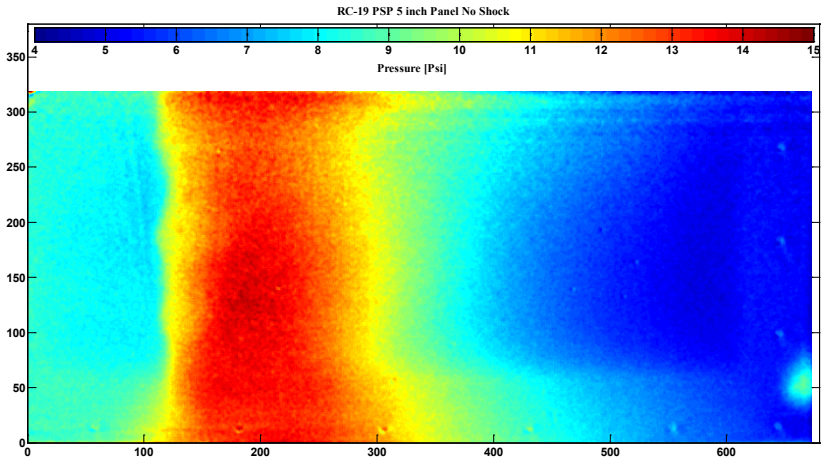

Figure 6. PSP Showing Shock Impingement Locations

a) no shock, b) shock at panel leading edge, c) shock near panel half length, d) shock at panel quarter length

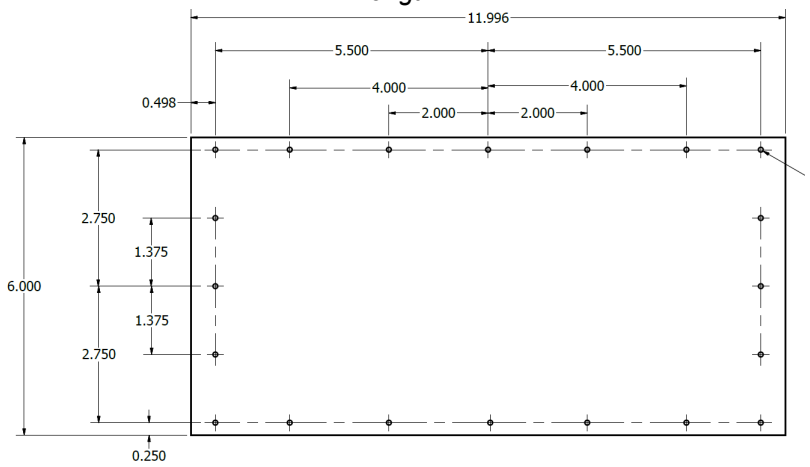

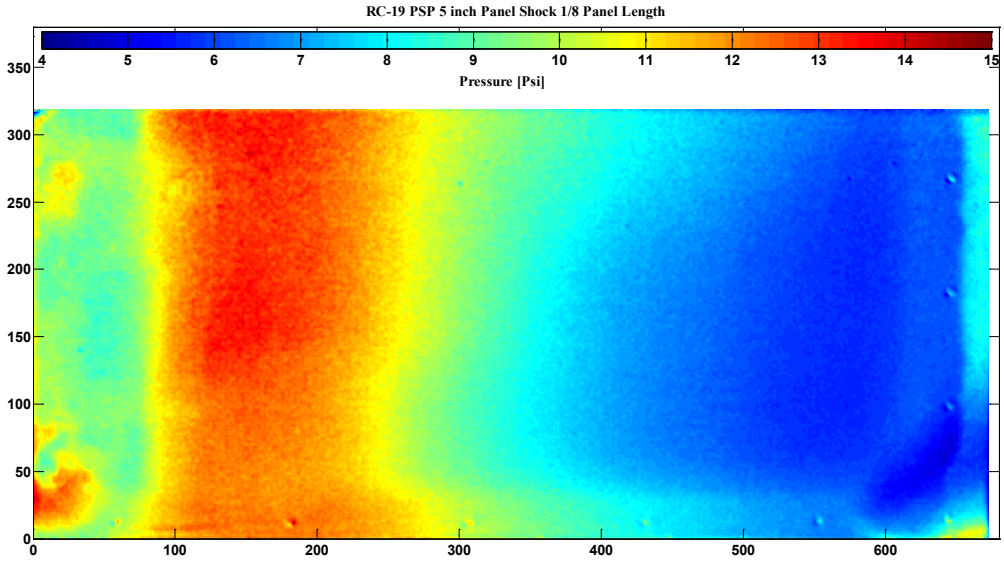

Figure 7. PSP Showing the Most Dynamic Panel Response Shock Impingement Location

The fast-reacting PSP results for a no-shock condition can be seen again in **Figure 8a**. Most of the 5- by 10-inch compliant panel is visible in the image. The darker regions on the edges of the image are part of the tunnel window frame and do not represent pressure on the panel. The variation in pressure across the panel for the no shock case is largely due to the dynamic movement of the panel into the flow. This interaction between compliant structure and high-speed flow can be further illustrated in **Figure 8b**. The pressure power spectral density (PSD) of a single pixel represented by the blue line and a 15- by 15-pixel averaged pressure are presented. It should be noted that a single pixel spans 0.4 mm and, therefore, a 15- by 15-pixel averaged area spans 6.2 mm. Two things are of particular note in the pressure PSD, 1) the peak in the pressure at 274 Hz occurs exactly at the first structural vibration bending mode frequency of the panel, and 2) the peak pressure becomes even more pronounced in the averaged data. In fact, taking a closer look at the average pressure data red line the second bending mode of the panel begins to emerge at approximately 350 Hz.

A couple of conclusions can be drawn from these results. First of all, the compliant panel's first bending mode is interacting with the high-speed flow to the extent that the panel is actually changing the flow indicating coupling. When the data is spatially averaged the interaction becomes more pronounced as the boundary layer pressure which is occurring on a rather small spatial scale is beginning to be filtered out of the pressure results and the large spatial scale plate modes effect on the flow become more prominent.

a)

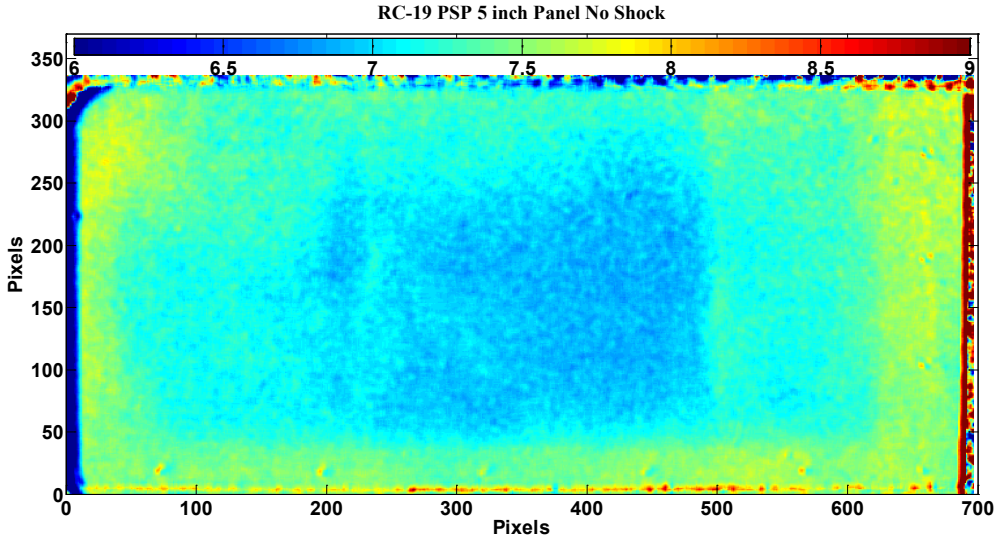

b)

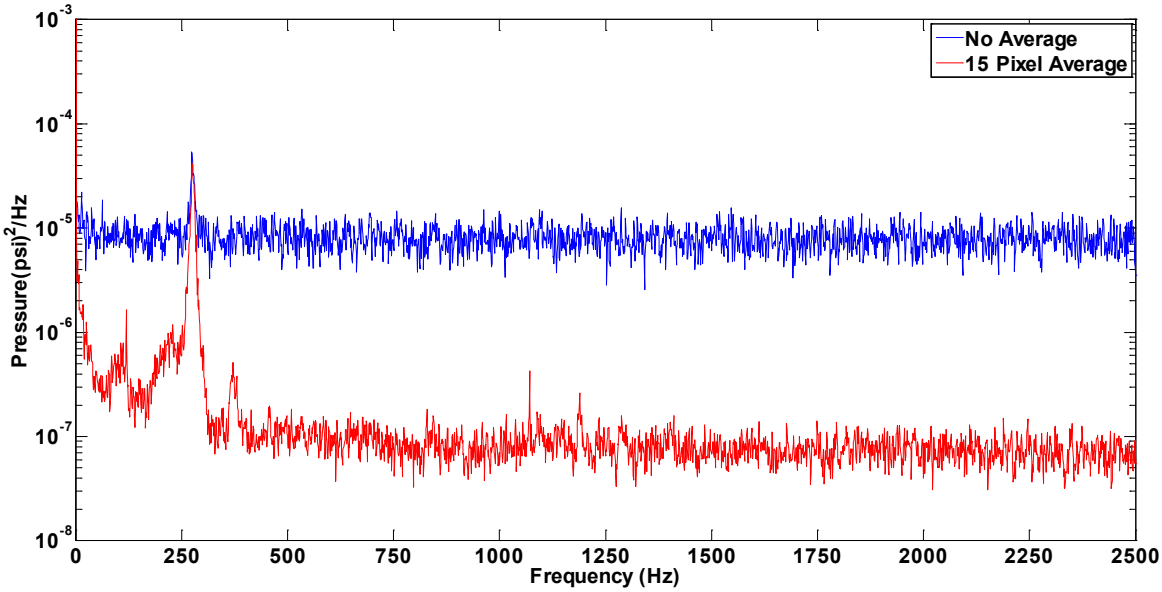

Figure 8. Fast-reacting PSP

a) single time increment full spatial plot and b) full time record single point pressure measurement PSD

This conclusion is further supported when the downstream Kulite pressure data is investigated in **Figure 9** as it nearly mirrors the 15- by 15-pixel spatially averaged PSP pressure results. It should be noted that given the magnitude of the Kulite pressure, the sensor area is actually approximately the size of a 9- by 9-pixel average area in the PSP. The size of the Kulite sensor head is 3.8 mm in diameter, which equates to about 9 pixels. This would indicate that the PSP can measure over a much smaller spatial area than more traditional sensors which means legacy turbulent boundary layer measurements were perhaps under reporting the true pressure magnitude.

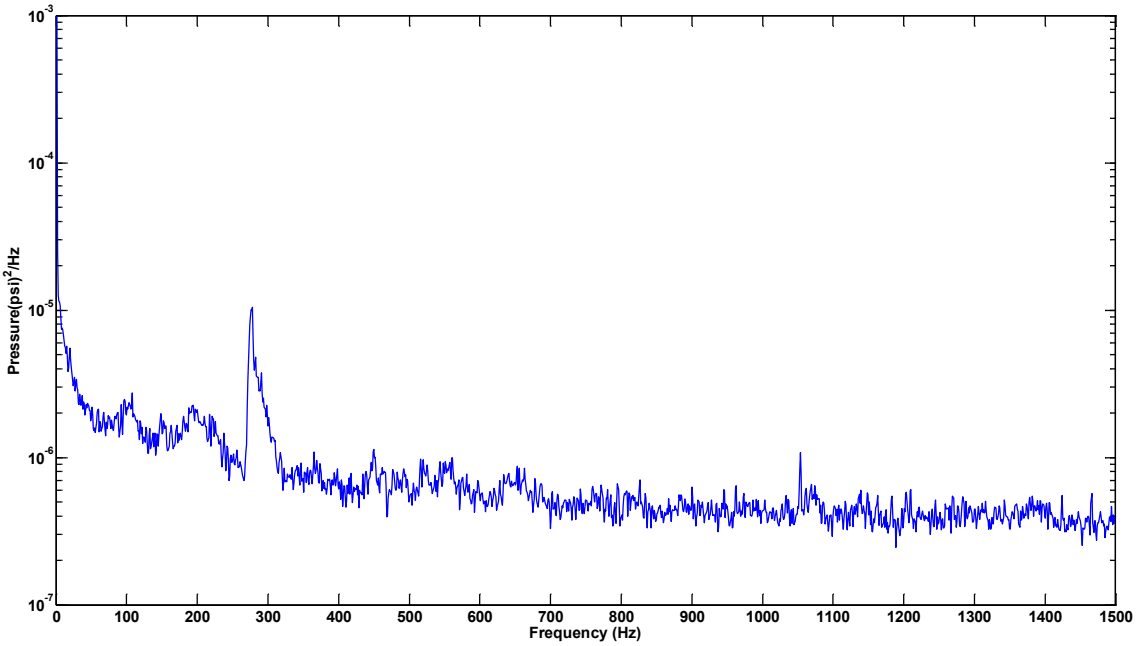

Figure 9. Kulite Wall Pressure Data Downstream of the Panel Showing Pressure Spike from Panel Vibration

3.3. Full Field Temperature

One of the findings from the previous effort was the need to acquire full field temperature measurement capability for the thin panel experiment. In the past, a thermocouple on the panel's frame and on the panel were used to ensure a small temperature difference indicating that the panel was in a thermal equilibrium.

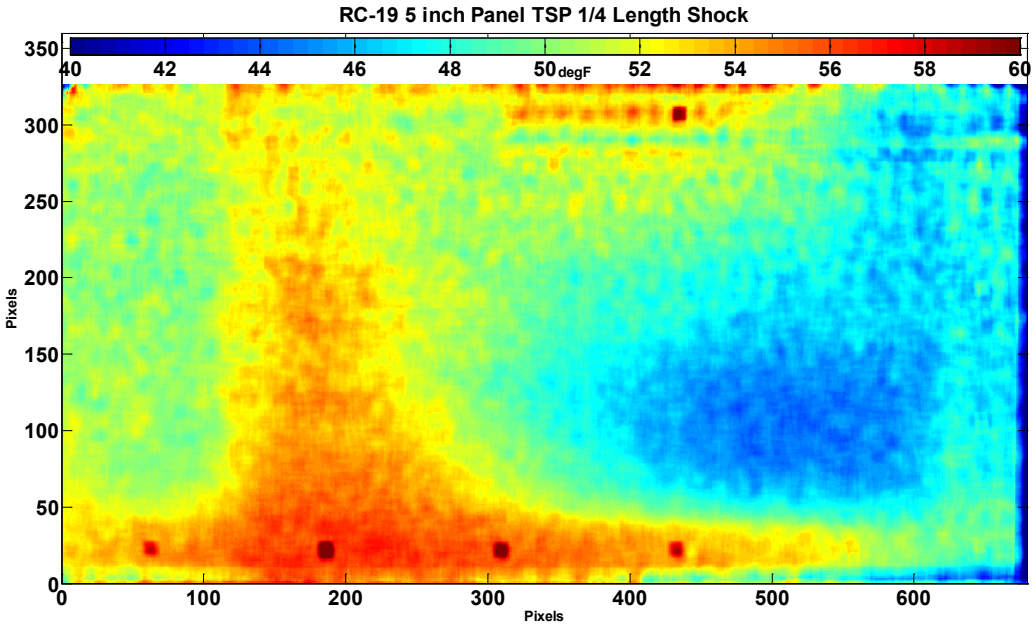

Figure 10. TSP Distribution for Shock Impingement
(quarter panel length case)

3.4. DIC Displacements and Strains

Unfortunately, calculated strains from DIC displacements tend to be noisy. Typical vibration displacements are near the limit of DIC measurement sensitivity [4]. Calculating strains from measurements so near the noise tend to amplify that noise making adequate strain results difficult to achieve. In past fluid-structure interaction (FSI) experiments, the focus was largely on the displacements, and any strain results were limited to the traditional foil strain gage at the center of the panel long edge. More recent experiments included thermal buckling with dynamic snap-through. Typically, buckled panel maximum displacements are more than twice as much as the unbuckled panel vibration displacements [5]. The fully buckled panel peak to peak displacements are on the order of 3 mm. For reference, the panel thickness is 0.63 mm. Considering the buckled panel displacements are so large, DIC strain results of the FSI experiment were thoroughly explored for the first time. See **Figures 11** and **12**.

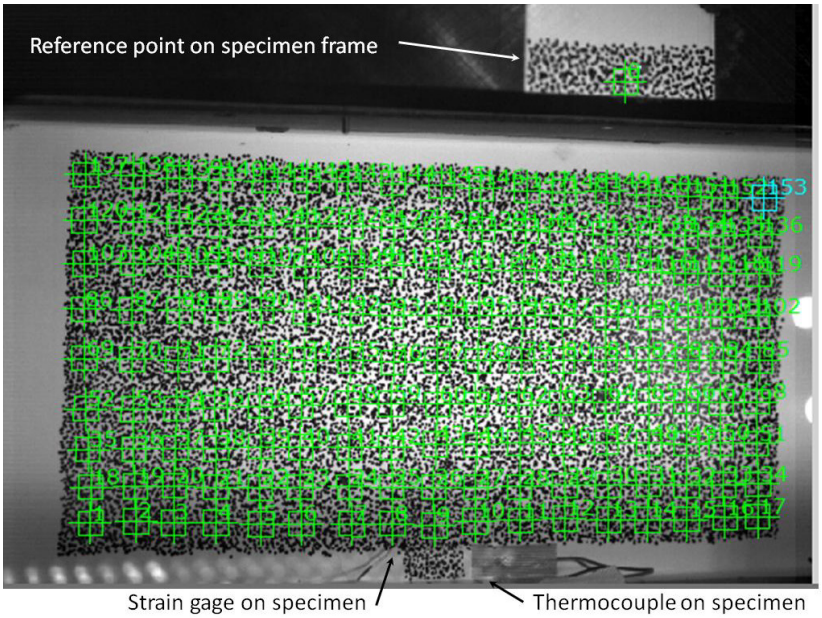

Figure 11. DIC Image of Panel with Facet Measurement Locations

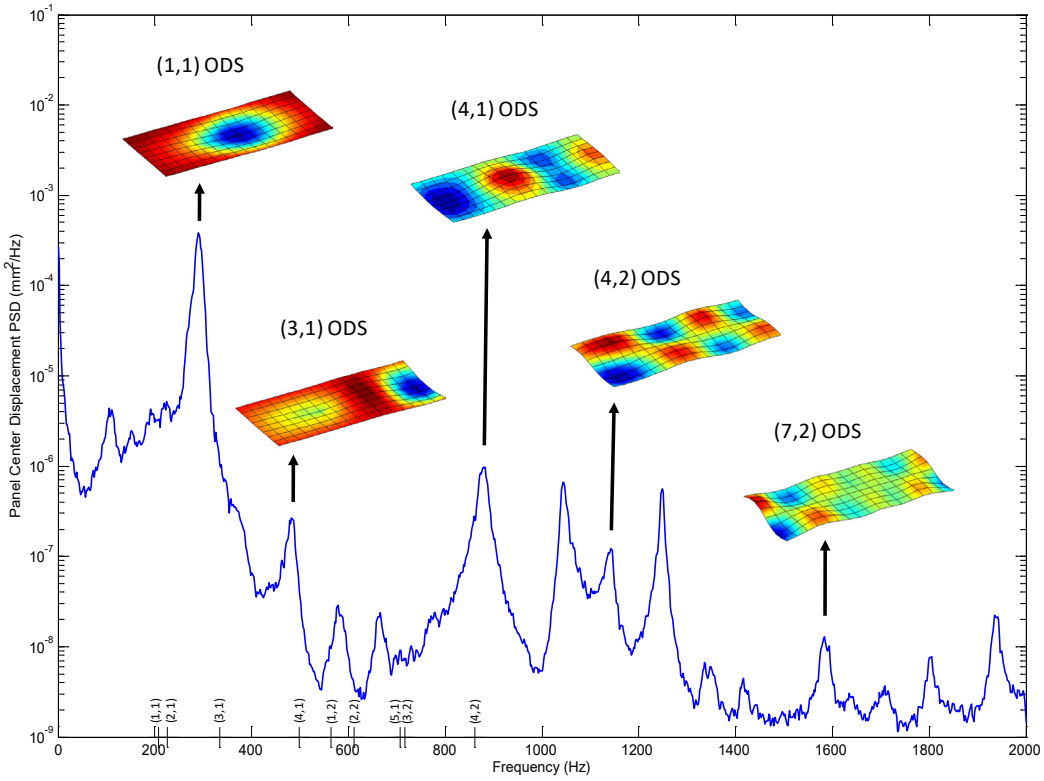

Figure 12. Panel Operational Reflected Shapes from DIC Results

The most dynamic unbuckled panel response once again occurred with a shockwave impingement at approximately 1/8 the panel length from the leading edge. **Figure 13** shows a qualitative comparison of a single moment in time full field displacement and resulting strain of the panel with a shock impingement. It is perhaps immediately apparent the increase in noise between the displacement in **Figure 13a** and the strain in **Figure 13b**. This panel response case is basically considered the lowest level random dynamic strain reasonably possible with high-speed DIC. **Figure 14** shows the time history and PSD of the panel strain along the stream wise centerline at discrete points near the leading edge, center line, and trailing edge. The root mean square (RMS) strains at the leading edge, centerline, and trailing edge are 134 με, 302 με, and 398 με, respectively. It can be seen from the PSD that the measurement noise floor is already beginning to limit the dynamic range at about 500 Hz, resulting in only the panel first mode being fully characterized.

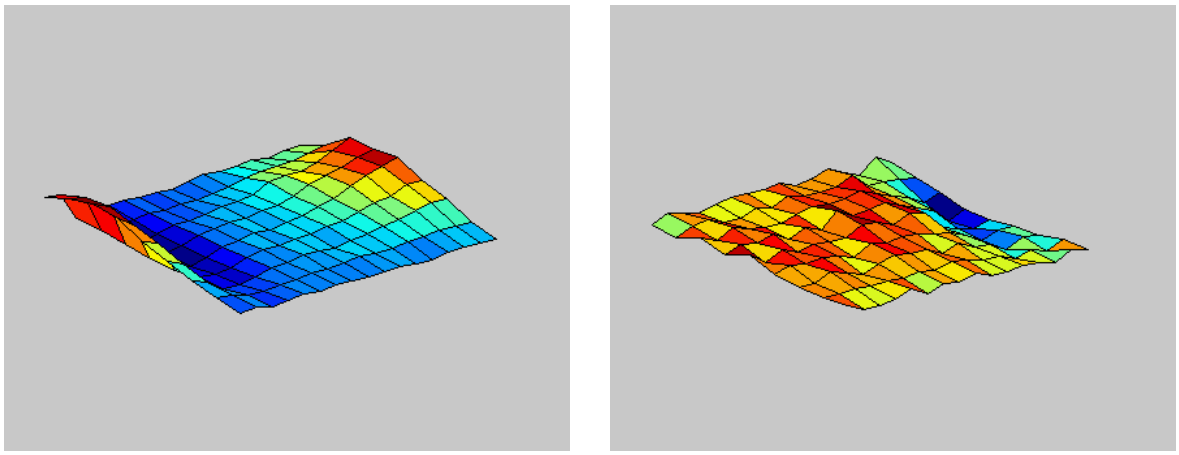

a) b)

Figure 13. Contour of Panel Response from a Shock Impingement at 1/8th Panel Length from Leading Edge
a) displacement (mm) and b) strain (με)

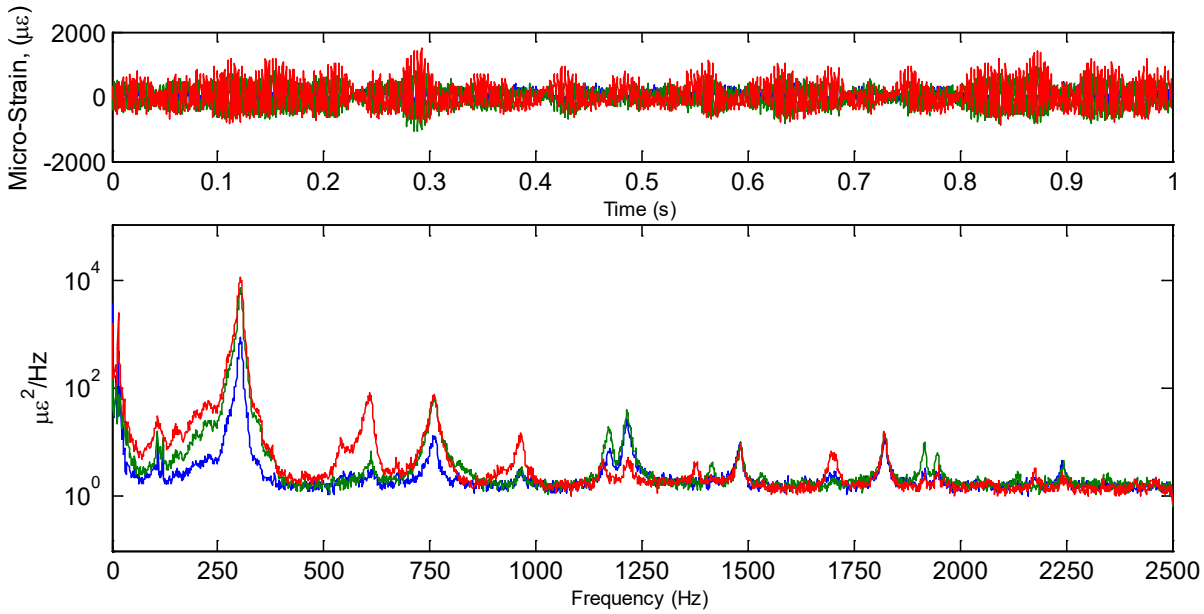

Figure 14. PSD Panel x-direction Strain
(-) leading edge, (-) centerline, and (-) trailing edge

The panel flutter condition displacement and strain contours can be seen in **Figure 15**. Clearly, the displacement levels are now at a level that make robust dynamic strain results possible. The strain PSD in **Figure 16** shows that the strains are now above the measurement noise floor all the way out to the 2,500 Hz Nyquist frequency. The strain RMS at the leading edge, centerline, and trailing edge are 2109 με, 1892 με, and 1491 με, respectively.

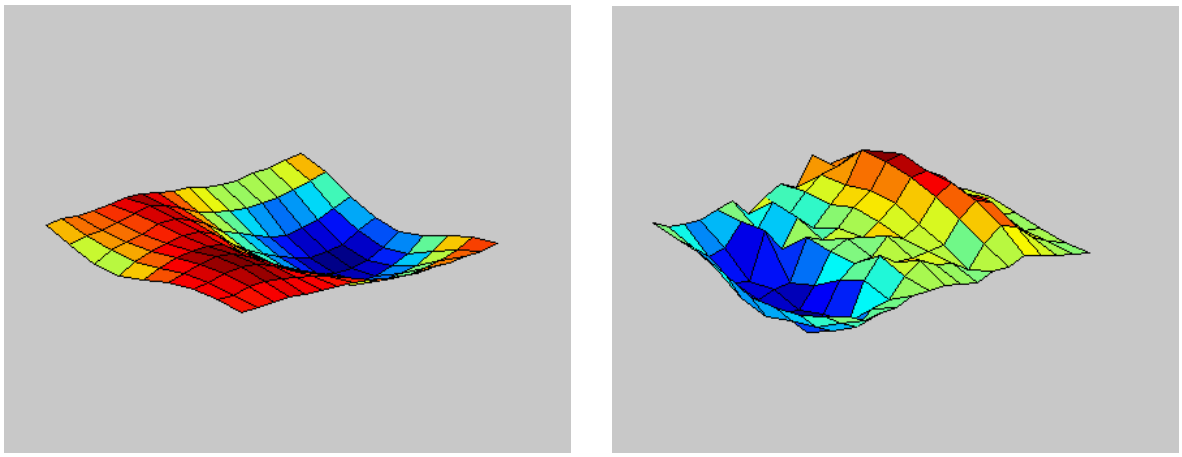

a) b)

Figure 15. Contour of Panel Response from First Thermal Condition Panel Flutter
a) displacement and b) strain

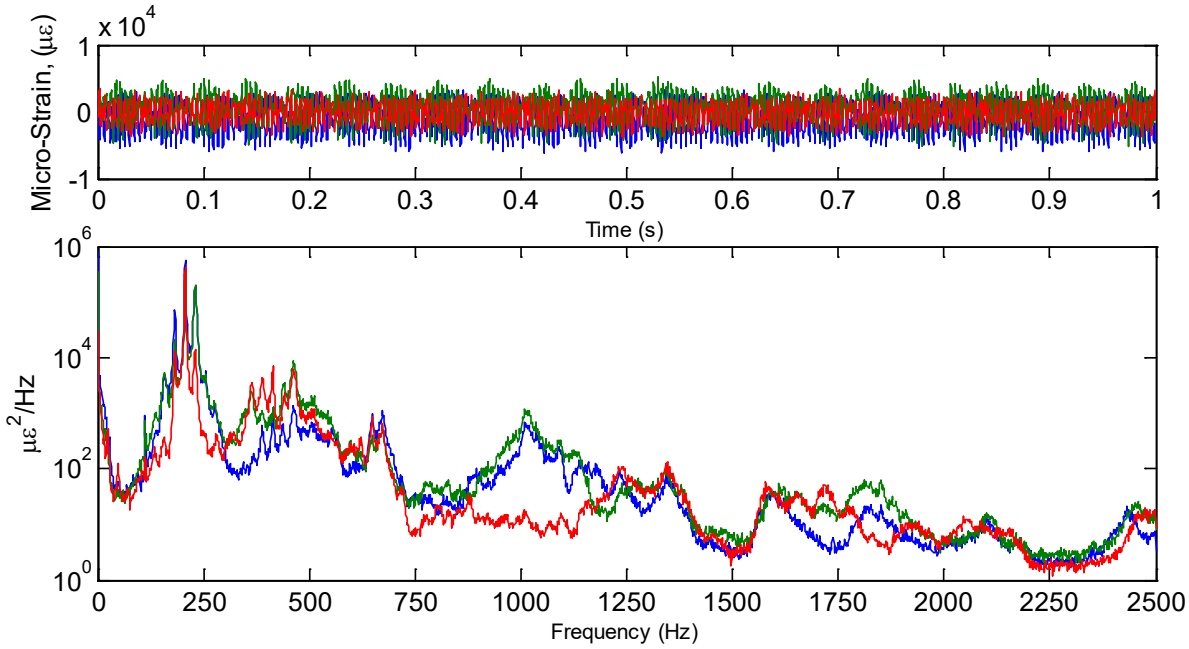

Figure 16. PSD of Panel x-direction Strain from Panel Flutter
(-) leading edge, (-) centerline, and (-) trailing edge

The panel thermal buckling condition displacement and strain contours are pictured in **Figure 17**. Shown is the stable buckled configuration that resembles the panel third linear mode shape. Shown is the stable buckled configuration that resembles the panel third linear mode shape; however, the shape is skewed due to the high-speed flow condition. The strain results are now well above the measurement noise floor. The strain PSD shown in **Figure 18** once again shows discrete point strain at the leading edge, centerline, and trailing edge. The buckled case PSD is 1/6th the time record of the previous cases in this study, demonstrating the potential lack of sufficient ensemble averages. The RMS strains at the leading edge, centerline, and trailing edge are 2093 με, 2685 με, and 1332 με, respectively. The RMS strains of both the flutter and buckled cases highlight a significant point.

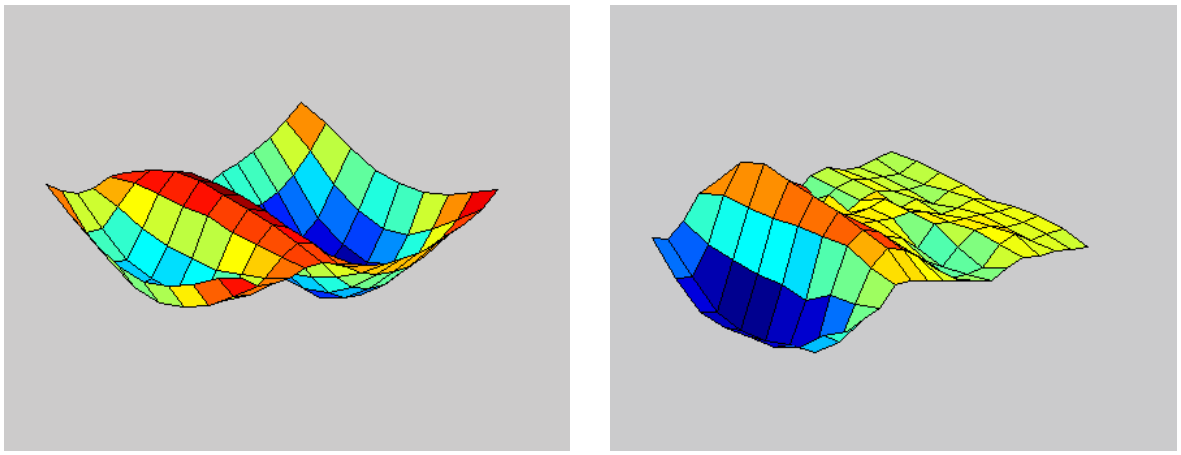

a) b)

Figure 17. Contour of Panel Response from Thermal Buckling
a) displacement and b) strain

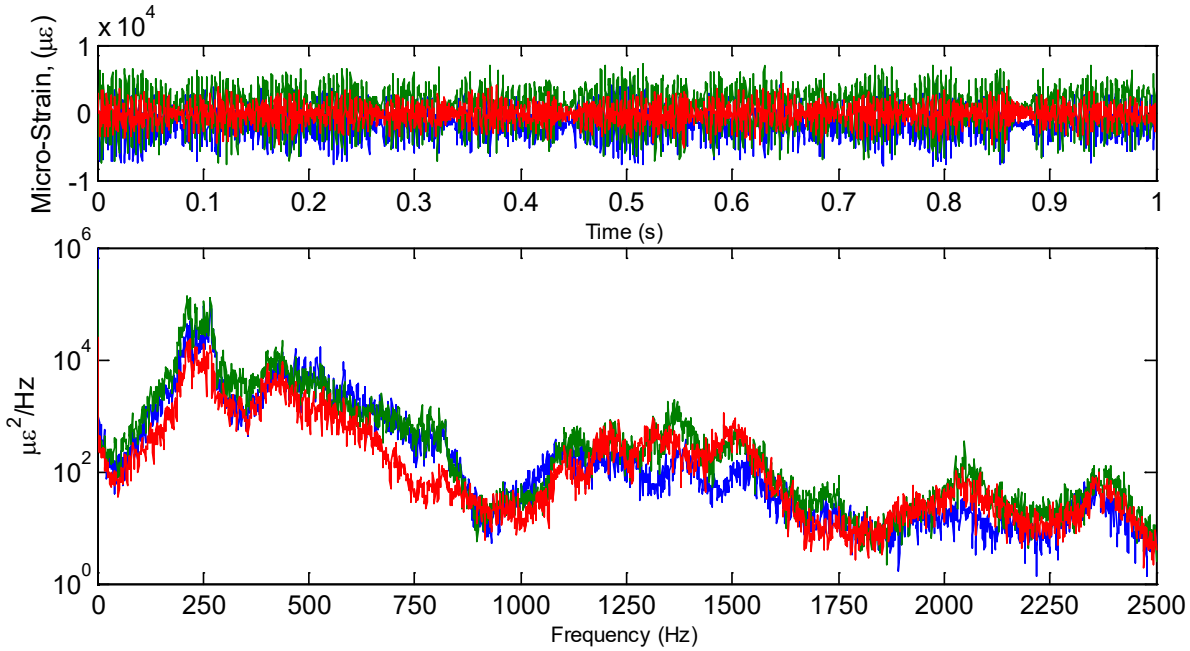

Figure 18. PSD Panel x-direction Strain from Thermal Buckling
(-) leading edge, (-) centerline, and (-) trailing edge

The strain levels experienced by the panel during the thermal cases are sufficient to result in high-cycle fatigue. The panel material is 4140 steel, which is the same material used in the wind tunnel test section. This panel specimen material was an attempt to avoid large coefficient of thermal expansion (CTE) differential between the tunnel walls and the panel.

Unfortunately, steel 4140 is a particularly strong material with an ultimate strength of approximately 1034 MPa. According to the DIC full field strain results the peak RMS strain experienced by the panel is equivalent to approximately 552 MPa. However, the 552 MPa loading experienced by the panel is accumulating cycles at about 250 Hz. Approximations of panel life at these loading levels would indicate the panel will crack and thus fail in less than 30 minutes of test time under these conditions.

To highlight the importance of the full field results obtained with high-speed 3D DIC, the discrete foil strain gage at the panel edge centerline for the same buckled panel test conditions measured only 1300 με. Based on the real-time foil gage results it was believed the strain the panel was experiencing was not of sufficient level and therefore it was decided the panel would not crack and fail and thus was not pursued. The DIC strain results indicated the panel should have failed in a relatively short period of time. Upon closer inspection of the panel post test, a crack was discovered along the trailing edge as seen in **Figure 19**.

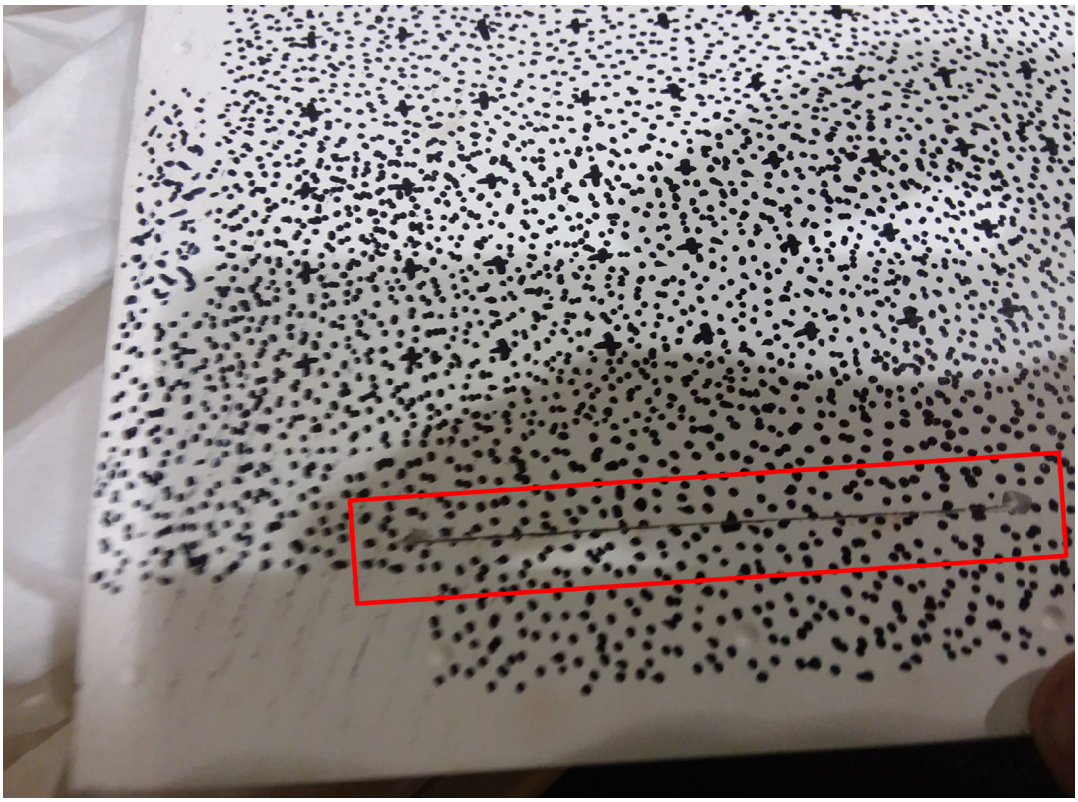

Figure 19. Image of Crack in Panel Specimen Trailing Edge

Further indication of high-speed fluid structure interaction can be seen in **Figure 20**. **Figure 20a** is the panel response at the center point with a shock impingement. It is a more typical and perhaps expected panel response to fluctuation pressure. **Figure 20b** is the same point response but with the shock impingement removed, producing what could be characterized as unexpected response. The response, although random and perhaps nonlinear, is similar in nature to a phenomena known as beating. When a lightly damped structure is given, a generally linear sinusoidal input at or near a fundamental frequency the input and the output of the specimen can couple and create linear combinations of harmonics of the fundamental frequency. The time signal will also display a consistent pulse looking response over time (beating). **Figure 20b** shows a nonlinear and random example of beating between the turbulent flow and the vibrating panel. The distinct lobes on either side of the first mode in the PSD and a pulsing-like behavior in the time signal in **Figure 20b** that is absent in **Figure 20a** represent the harmonics. The flow and the panel are exchanging energy back and forth at the panel's first bending mode frequency adding further evidence that strong fluid structure coupling has been demonstrated.

a)

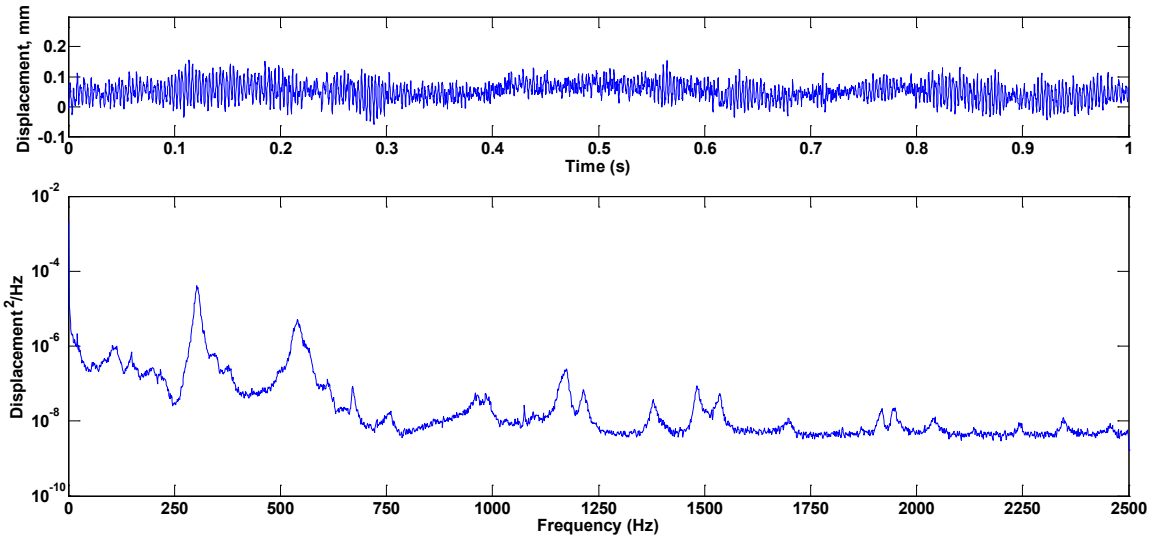

b)

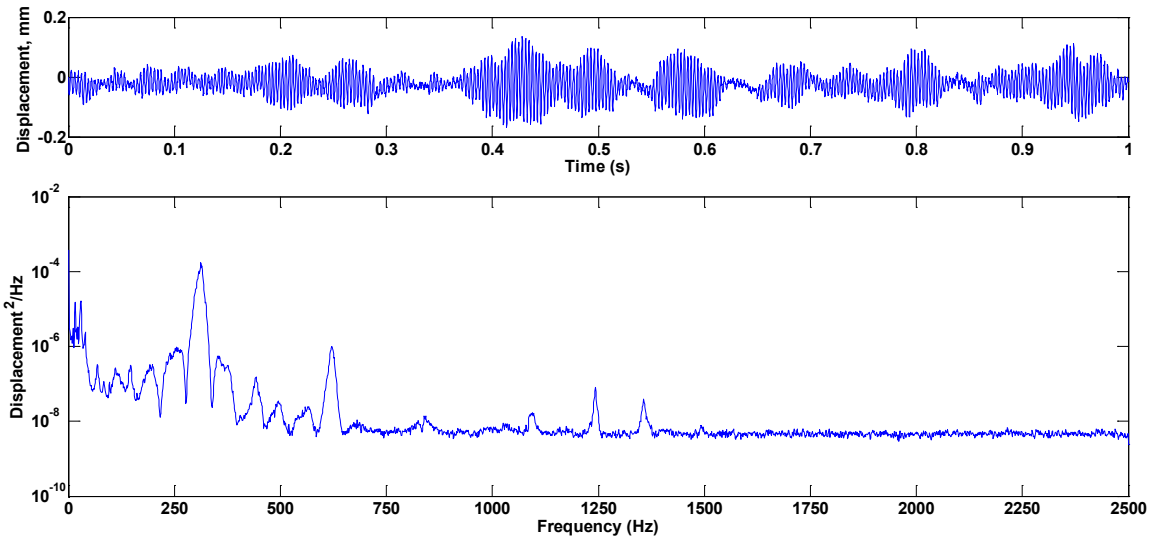

Figure 20. Compliant Panel Transverse Vibration Response Near Center Point
a) with a shock impingement and b) no shock impingement indicating "beating"

As it was mentioned previously, DIC has traditionally been recorded from the backside of the panel specimen in the RC-19 fluid structure interaction studies which means there is essentially no flow across the image. Speculation has run high that filming DIC through high-speed flow, and, more importantly, an oblique shockwave with the high density gradients, could distort the image to the point that the DIC displacement results would be adversely affected. Referring back to **Figure 1b**, a second set of DIC cameras were included in a set of experiments to simultaneously film DIC images from both the traditional back non-flow side and the front flow side of the panel. It has been noted that in some high-speed tunnel facilities, filming a specimen from the non-flow side would be impossible without significant tunnel test section modification. Because of the extensive optical access provided by the RC-19 facility, the opportunity to do a thorough comparison between flow and no flow DIC was possible.

When comparing the DIC displacement results of the front flow side at various locations in **Figure 21**, it can be seen that the results are, in fact, affected by the shockwave. Shown is a solid blank specimen and any major peaks are the rigid body vibrations of the tunnel. The very large peak at about 20 Hz is the tunnel first bending mode in the vertical direction which was confirmed with an impact hammer modal test of the wind tunnel test section.

The dual DIC test was repeated with the flexible specimen; however, currently the blank specimen results are only presented for clarity. The blue line is the no shock case and is considered a baseline noise measurement for DIC through high-speed flow. The green line representing the reflected shock is very similar to the no shock case, leading to the conclusion that the reflected shock has little to no effect on the DIC results. However, when looking at a DIC point through the upstream incident shock, the results change rather significantly. The same general increase in dynamic content that was seen in the shockwave motion can be seen at lower frequencies in the DIC. In general, the sharp density gradient of the incident shock increases the DIC measurement noise and in particular at frequencies below 1000 Hz. Future work will investigate if given the shockwave dynamic motion results provided by the high-speed shadowgraph in **Figure 4**, that a correction to the DIC distorted results could perhaps be accomplished when filming through a shockwave is unavoidable.

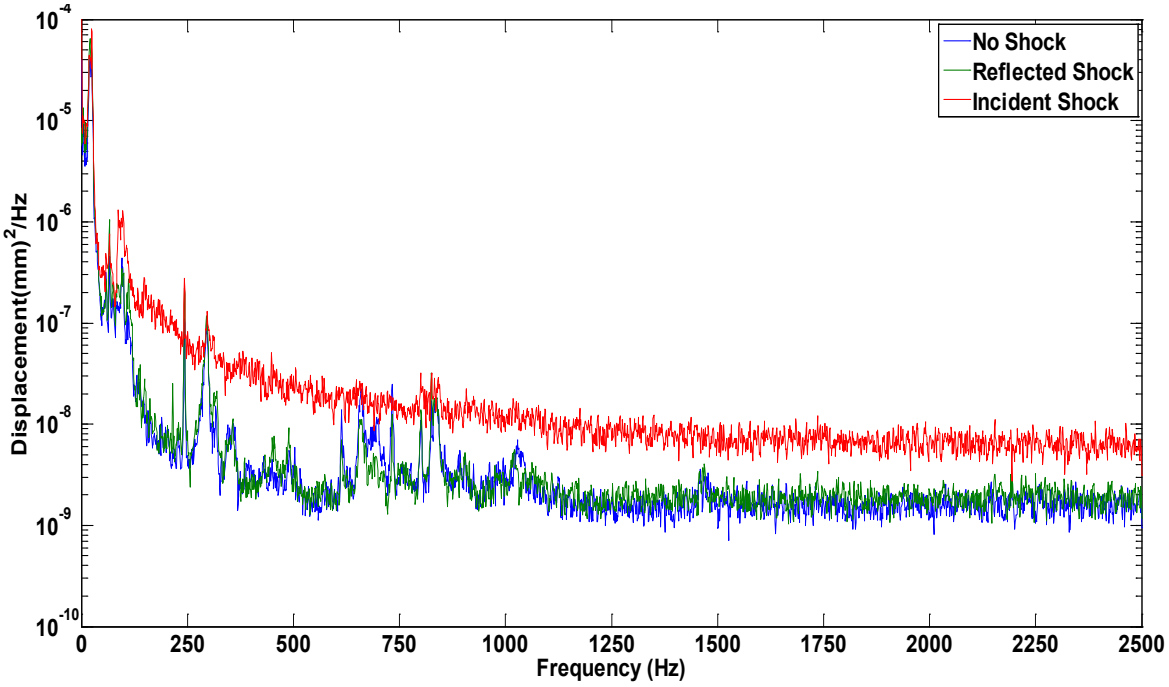

Figure 21. PSD of DIC Displacement of a Rigid Blank Specimen

(▬) no shock, (▬) reflected shock, and (▬) incident shock

Coupled Modeling Methods – Exploration of the fluid-thermal-structural coupling requirements and characteristics necessary to predict the response and life of a structure with transient and dynamic loading, exhibited in the RC19 thin panel experiment were pursued. These evolving methods were integrated into simulations of the experiment to investigate sensitivities of parameters that could be controlled in the experiment. This investigation helped identify the need to control the back pressure on the panel. Previously the cavity pressure was measured with static and dynamic gages but not controlled. The cavity occurs between the thin panel's non-flow side and the window for DIC viewing and was vented to tunnel conditions downstream of the thin panel. This is necessary to prevent the yielding of the panel during

tunnel startup where a vacuum of approximately 3 psi is used. The current venting system was altered to allow for venting that can be closed off after startup along with a way to control the cavity pressure once flow is established in the tunnel. Additionally, other areas that were identified as important were the boundary layer thickness, thickness variation in the panel, temperature variation in the panel, and the need to anchor the fast-reacting PSP, to more traditional measurement techniques such as Kulites and microphones. This information reflected in the modifications to the experiment and test plan. An example simulation of the RC19 thin panel experiment is shown in **Figure 22**, in which a PSD of deflection is shown against frequency for the previously acquired data. This work was leveraged from Prof. McNamara's group at Ohio State.

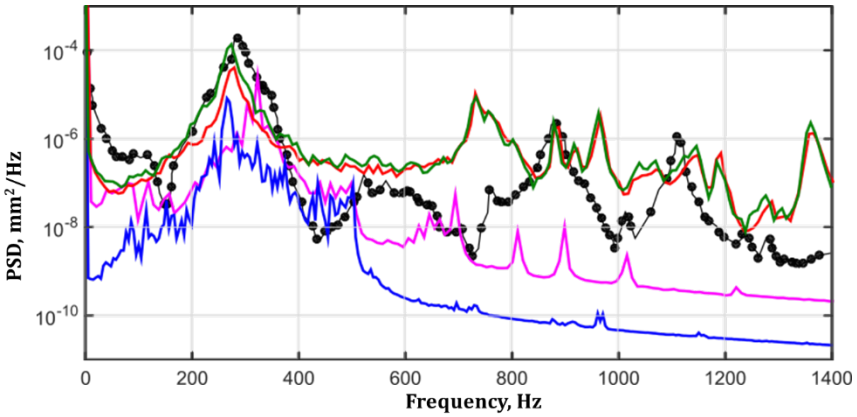

Figure 12. PSD of Deflection
(black line with black glyphs denote experiment and color lines denote simulation results with differing shock and pressure correlation assumptions)

Enabling Long-Duration Time-Record Simulations – A variable-fidelity simulation framework is being pursued, incorporating both coarse-scale and high-fidelity features through hierarchical enrichments in regions of local high gradients. Specific focus has been given to locally high stress regions in the flexible panel in an attempt to predict acoustic fatigue failure. Current work focuses on verifying and validating generalized finite element methods (GFEM). This method has been used to capture the spatial temperature distribution on structures from shock impingement as well as the distribution of stress around the crack tip. To demonstrate the ability of the process to track an evolving fine scale feature in coarse scale, a fatigue crack simulation was performed along with experimental testing to validate the developed methods. Several crack orientations were utilized to test the robustness, as shown in **Figure 23**. Data from experiment and simulations is shown in **Figure 24** for the double vertical slot configuration along with the 90th percentile.

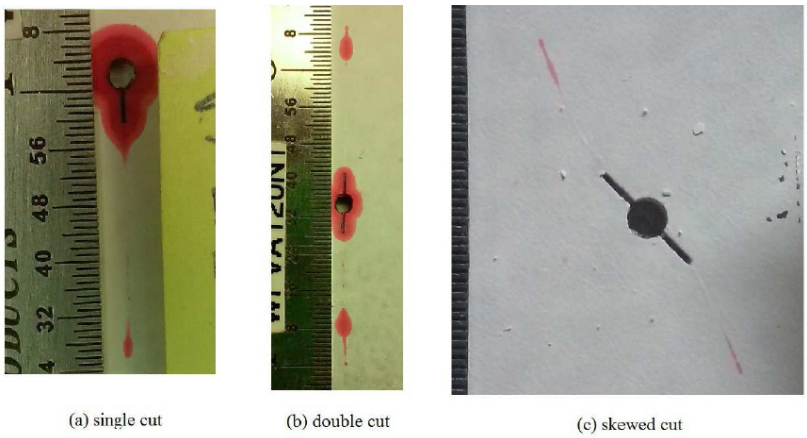

Figure 22. Initial Crack Orientations Used to Validate the GFEM Code

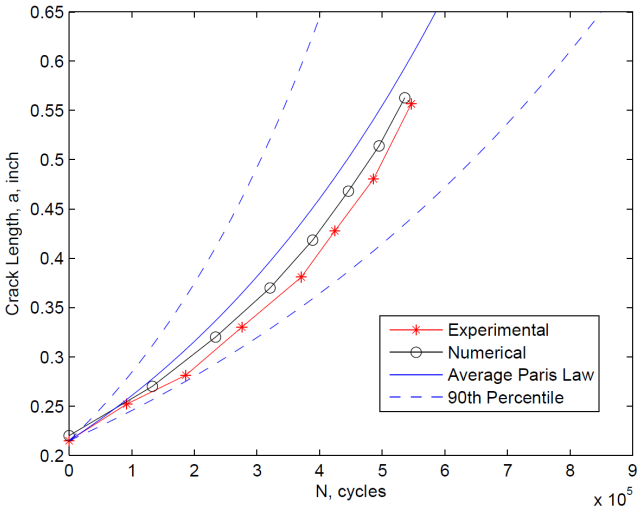

Figure 24. Initial Crack Orientations Used to Validate the GFEM Code

4. Conclusions

A high-speed FSI study was conducted in a Mach 2 wind tunnel with various shock impingement scenarios explored on a flexible panel. Full-field panel temperature measurement and shockwave high-speed shadowgraph were added to the experiment to supply additional desired information for coupled model development. Further evidence of full-fluid structure coupling was successfully captured across multiple types of measurements. Of particular interest in the latest series of experiments was the possible effects of filming DIC vibration measurement of the flexible panel through the shockwave. Therefore, effects of the steep density gradients associated with high-speed flow shockwaves was investigated. Results indicate that full-field optical vibration measurement techniques such as high-speed 3D DIC results can be adversely affected by distortion in the images. The effects and possible causes of distortion was further demonstrated with high-speed shadowgraph showing the dynamic movement of the shockwave. Future work will include exploring possible corrections for the distorted DIC displacement results.

Most recently, a study of the strain results from thermal buckling of the panel was undertaken. In previous tests, the noise associated with the high-speed 3D DIC strain results made a study of the full-field strain difficult if not unproductive. With the addition of thermal buckling to the test procedure, sufficient levels of displacements and, therefore, strain were achieved to make a full-field strain analysis feasible. Results indicate that not only were the random dynamic strain levels large enough to be quantified by DIC, but also were of a sufficient level to induce high-cycle fatigue failure despite the traditional foil strain gage levels well below the panel yield strength. Initial fatigue predictions of the panel based on the maximum strains measured with DIC indicate that the panel would fail in a relatively short test time of approximately 30 minutes. Closer inspection of the panel posttest revealed that the panel had indeed cracked along its trailing edge near the end of the testing. Therefore, the series of tests were deemed a success and the resulting test data will be disseminated to the fluid-structure modeling community for validation purposes.

5. REFERENCES

[1] B. Zuchowski, "Predictive Capability for Hypersonic Structural Response and Life Prediction, Phase 1 – Identification of Knowledge Gaps," Technical Report, AFRL-RB-WP-TR-2010-3069, August 2010.

[2] T. Beberniss, S. Spottswood, and T. Eason, "High-Speed Digital Image Correlation Measurements of Random Nonlinear Dynamic Response," SEM Annual Conference, Uncasville, CT, June 10-13, 2011.

[3] S. Spottswood, T. Eason, and T. Beberniss, "Influence of Shock-Boundary Layer Interactions on the Dynamic Response of a Flexible Panel," ISMA Biennial Conference on Noise and Vibration Engineering, Leuven Belgium, 2012.

[4] T. Beberniss, S. Spottswood, and T. Eason, "High-Speed 3D digital image correlation measurements of long-duration random vibration; recent advancements and noted limitations," ISMA Biennial Conference, Lueven, Belgium, September, 2012.

[5] T. Beberniss, S. Spottswood, D. Ehrhardt, and R. Perez, "Dynamic Response of a Thin Panel Subjected to a Shock Wave Impingement and Thermal Buckling," AIAA Aviation Conference, Denver, CO, June 2017.

[6] M.R. Gruber, A.S. Nejad, "Development of a Large-Scale Supersonic Combustion Research Facility," 32nd Aerospace Sciences Meeting & Exhibit, Reno, NV, January 1-13, 1994, AIAA Paper 94-0544.

5.1. Collaborations

Prof. Jack McNamara, The Ohio State University: Improved Understanding of Shock Boundary-Layer Interaction (SBLI) for High-Speed Flows Over Compliant (Deforming) Panels Using High-Fidelity-Informed Fluid Models

Prof. Matt Allen, The University of Wisconsin-Madison: Substructuring with Nonlinear Subcomponent Models Based on Nonlinear Normal Modes with Application to Hypersonic Vehicle Design

Prof. Lawrie Virgin, Duke University & Prof. Ilinca Stanciulescu, Rice University: *Snap-through and Thermal Buckling, a Combined Experimental and Numerical Study*

Prof. Marc Mignolet: Thermoelastic Reduced Order Models (ROMs) for Representative Hypersonic Structures

5.2. Publications

T. Beberniss and D. Ehrhardt, "High-Speed 3D Digital Image Correlation Vibration Measurement; Recent Advancements and Noted Limitations," *Journal of Mechanical Systems and Signal Processing*, Volume 86, March 2016, Pages 35-48.

T. Beberniss, S.M. Spottswood, and D. Ehrhardt, "Nonlinear Response of a Thin Panel Subjected to a Shockwave Impingement," SEM International Modal Analysis Conference, Orange Grove, CA, USA, February, 2017.

T. Beberniss, S.M. Spottswood, R. Perez, D. Ehrhardt, and T. Eason, "Dynamic Response of a Thin Panel Subjected to a Shockwave Impingement and Thermal Buckling," AIAA Aviation Conference, Denver, CO, USA, June, 2017.

T. Beberniss and D. Ehrhardt, “Temporal Aliasing in High-Speed 3-Dimensinoal Digital Image Correlation Vibration Measurements,” AIAA SciTech Conference 2015; Kissimmee, FL, USA, January 5-9, 2015; AIAA-2015-2059.

A. Gogulapati, R. Deshmukh, J. McNamara, V. Vyas, X. Wang, M. Mignolet, T. Beberniss, S. Spottswood, and T. Eason, “Response of a Panel to Shock Impingement: Modeling and Comparison with Experiments – Part 2,” AIAA SciTech Conference 2015; Kissimmee, FL, USA, January 5-9, 2015, AIAA 2015-0685.

P. O’Hara, J. Hollkamp, C.A. Duarte, and T. Eason, “A Two-Scale Generalized Finite Element Method for Fatigue Crack Propagation Simulations Utilizing a Fixed, Coarse Hexahedral Mesh,” *Computational Mechanics*, Volume 57(1), 2015, Pages 55-74, Doi:10.1007/s00466-015-1221-7

P. O’Hara, P. Gupta, and C.A. Duarte, “Application of the Generalized Finite Element Method to Crack Coalescence Simulations Utilizing Fixed, Coarse Finite Element Meshes.” United States National Congress on Computational Mechanics 13; San Diego, CA, USA, July 26-30, 2015.

P. O’Hara, C.A. Duarte, and T. Eason, “A Two-Scale Generalized Finite Element Method for Linear Elastic Fracture Mechanics Analyses Utilizing Fixed, Coarse Hexahedral Meshes.” Pan-American Congress of Applied Mechanics XV; Champaign, IL, USA, May 18-21, 2015.

LIST OF ACRONYMS, ABBREVIATIONS, AND SYMBOLS

ACRONYM	DESCRIPTION
3D	three dimensional
CTE	coefficient of thermal expansion
DIC	digital image correlation
FSI	fluid-structure interaction
GFEM	generalized finite element methods
PSD	power spectral density
PSP	pressure sensitive paint
RMS	root mean square
TSP	temperature sensitive paint